Photochemistry of Iron in Simulated Crustal Aerosols with Dimethyl Sulfide Oxidation Products

ARTICLE *in* ENVIRONMENTAL SCIENCE AND TECHNOLOGY · FEBRUARY 2008

Impact Factor: 5.33 · DOI: 10.1021/es071469y · Source: PubMed

Photochemistry of Iron in Simulated Crustal Aerosols with Dimethyl Sulfide Oxidation Products

JENNIFER M. KEY, NICOLE PAULK, AND ANNE M. JOHANSEN*

Department of Chemistry, Central Washington University, 400 East University Way, Ellensburg, Washington 98926

Received June 16, 2007. Revised manuscript received September 11, 2007. Accepted September 13, 2007.

Iron contained in dust-derived aerosol particles deposited into remote oceans is essential for phytoplankton productivity, which controls photosynthesis rate and the uptake and release of climate forcing gases. Understanding chemical mechanisms that control iron bioavailability, that is, its speciation, is therefore crucial for global climate predictions. In the present study, the photoredox chemistry of iron in marine atmospheric aerosol particles was investigated by using ferrihydrite as a surrogate iron phase in the presence of dimethyl sulfide (DMS) derived oxidation products: dimethyl sulfoxide (DMSO), dimethyl sulfone ($DMSO_2$), methane sulfinic acid (MSIA), and methane sulfonic acid (MSA). Reactants and products were analyzed with UV–vis absorption spectroscopy, ion chromatography, and a hydrogen peroxide sensitive electrode. Results show that MSIA enhances the photoreductive dissolution of iron in a ligand-to-metal charge transfer reaction producing Fe(II), MSA, and H_2O_2. The rate law for Fe(II) is close to first order (0.79) with regard to adsorbed MSIA and has an empirical rate constant of 1.4×10^{-4} s^{-1}. This mechanism may represent a significant pathway through which iron becomes more bioavailable, and it contributes to models of iron and sulfur chemistries in the marine atmosphere.

Introduction

Iron (Fe) is an essential micronutrient necessary for the metabolic processes (e.g., photosynthesis and cellular respiration) of marine phytoplankton. In open-ocean environments, far from continental shelves and upwelling currents, iron availability is limited primarily to the atmospheric deposition of crustal-derived aerosols that have been transported to sea by prevailing winds (*1*). Bioavailability to phytoplankton is further limited mostly to the soluble fraction of iron, consisting of Fe(II) and minute concentrations of dissolved and organically complexed Fe(III) (*2*). Marine microorganisms have adapted specialized alternative mechanisms to acquire the more abundant but only sparingly soluble colloidal iron(oxy)hydroxides, which are thermodynamically the most stable chemical forms of iron in oxygenated marine environments (*3*). In particular, some organisms synthesize and release low molecular weight ligands that have a high binding affinity for Fe(III), that is, siderophores, into their surroundings (*4*) to capture iron for their metabolic needs. This siderophore production requires a considerable expenditure of both energy and materials and is therefore typically only prevalent when organisms are under stress (e.g., due to iron limitation) (*5*). In another important process precipitated Fe(III) is converted to the more bioavailable dissolved Fe(II) through photoinduced ligand-to-metal charge transfer (LMCT) between carboxylic acid moieties of organic compounds complexed to Fe(III) (*6, 7*). LMCT occurs, for example, between Fe(III) and oxalate ($C_2O_4^{2-}$), a final product from the oxidation of organic pollutants present in cloud and fogwater (*8*), and between Fe(III) and α-hydroxycarboxylate groups of siderophores (*4*). Although $Fe(OH)^{2+}$ itself undergoes photolysis to produce Fe(II), the presence of a ligand lowers the energy necessary for Fe(III) reduction and shifts the spectrum of light absorption to longer wavelengths into the visible region of the solar spectrum, thus increasing the rate of iron reduction. While this type of LMCT reaction may be a significant source of Fe(II) in surface waters after atmospheric deposition, recent laboratory observations have shown that in the remote marine atmosphere a biogenically mediated LMCT reaction may further enhance iron bioavailability in crustal particles (*9*). This mechanism is controlled by oxidation products of dimethyl sulfide (DMS) that is released from phytoplankton when under oxidative stress, such as caused by iron limitation or increased UV radiation (*10*), and thus establishes a biogeochemical link between phytoplankton and iron bioavailability.

Although DMS oxidation in the gas and liquid phases has been extensively studied and modeled (*11–13*) because of its ability to form cloud condensation nuclei (CCN) and affect the global climate (*14*), its relationship to iron chemistry is recent (*9*) and constitutes the focus of the present study. The photochemical dissolution of ferrihydrite, the most likely form of iron found in weathered and reprocessed aerosol particles (*15*), is investigated in the presence of DMS oxidation intermediates including dimethyl sulfoxide (DMSO, $CH_3S^{(0)}OCH_3$), dimethyl sulfone ($DMSO_2$, $CH_3S^{(2+)}O_2CH_3$), methane sulfinic acid (MSIA, $CH_3S^{(2+)}O_2H$), and methane sulfonic acid (MSA, $CH_3S^{(4+)}O_3H$). Mechanistic information revealed in the present study will likely fill gaps in currently incomplete atmospheric iron and sulfur chemistry models over the oceans and thus contribute to global climate prediction (*13, 16, 17*).

Experimental Section

Reagents and Standards. Photochemical dissolution experiments were carried out with amorphous ferrihydrite in the presence of DMS-derived sulfur species (i.e., DMS (98%, Sigma-Aldrich), DMSO (99.9%, Sigma-Aldrich), $DMSO_2$ (98.0%, Alfa Aesar), sodium salt of MSIA (97.0%, Lancaster), and MSA (99.0%, Sigma-Aldrich)). Unless otherwise noted, ferrihydrite was synthesized from iron perchlorate, $Fe(ClO_4)_3 \cdot 6H_2O$ (Reagent grade, Alfa Aesar) using a method described by Schwertmann and Cornell (*15*), where the iron hydroxy–polymer suspension was dialyzed and freeze-dried. Powder X-ray diffraction (XRD) was used to confirm the amorphous nature of the ferrihydrite and establish that there were no significant crystallographic differences between batches before and after the experiment (see Supporting Information Figure 1 for an example scan). The ground-up ferrihydrite crystals had a consistent specific surface area of $\sim 200 \pm 10$ m^2 g^{-1} as determined by the BET method (FlowSorb III, Micromeritics, model 2305) (*18*). Batches of ferrihydrite were stored dry and dark at −30 °C. Transformation of ferrihydrite to more crystalline phases during storage over the 1–2 months that it took to perform sets of experiments was not observed on the XRD.

* Corresponding author phone: (509) 963-2164; fax: (509) 963-1050; e-mail: johansea@cwu.edu.

10.1021/es071469y CCC: $40.75
Published on Web 11/30/2007

TABLE 1. Simulated and Reported Open Ocean Atmospheric Fe- And S-Species Concentrations of Relevance

compound (gas or particulate)	reaction medium concentration (mM)	simulated[a] atmospheric concentration (nmol (m^3 air)$^{-1}$)	remote open ocean atmospheric concentration (nmol (m^3 air)$^{-1}$)	references
ferrihydrite	0.25 g	2.5[b]	2.3	(*22, 23*)
DMS(g)	N/A	N/A	3.9–13.1	(*25, 26*)
DMSO(g)	N/A	N/A	0.06–3.6	(*27–29*)
DMSO(p)	35	3.5	0.001–0.125	(*25, 30*)
$DMSO_2$(g)	N/A	N/A	0.053	(*28, 31*)
$DMSO_2$(p)	7.4	0.74	not reported	
MSIA(p)	0.01–1.3	0.001–0.13	not reported	
MSA(p)	0.62	0.062	0.01–0.8	(*24, 26, 32, 33*)

[a] Assuming an atmospheric liquid water content of 1.0×10^{-10} m^3 aq (m^3 air)$^{-1}$ (*21*) and a reaction volume of 0.1 L. [b] Assuming 25% of Fe(tot) in the atmosphere is ferrihydrite.

Experimental Setup. Sunlight was simulated with a 1000 W ozone-free Xenon lamp (Thermo Oriel). The light was focused by a condensing lens, passed through an IR filter and two sequential air mass filters (AM 0 and AM 1, Newport Corp.), and redirected by a beam turner onto the reaction vessel. Filters served to simulate the solar spectrum at ground level at the equator when the sun is directly overhead, but potassium ferrioxalate actinometry (*19*) revealed an incident light intensity (I_0) of 1.2 kW m^{-2}, comparable to sunlight intensity from 300 to 500 nm at noon during summer at mid-latitude (*20*).

Reactants were added directly to 0.100 L of Milli-Q water ($R = 18$ MΩ cm) in a 250 mL temperature controlled (20.0 °C) water-jacketed Pyrex reaction vessel (irradiated surface area, 20.3 cm^2). This volume is representative of 1.0×10^6 m^3 air with a liquid water content of 1×10^{-10} m^3 aq (m^3 air)$^{-1}$ (*21*). Initial concentrations of added species are presented in Table 1, both in the reaction medium, representing the liquid aerosol phase, and in the projected air volume. For comparison, reported values of species in marine air are also listed. Ferrihydrite was estimated at 25% (*22, 23*) of total iron observed over the remote ocean (*24*); thus, 0.25 g of ground ferrihydrite was added to the reaction medium. Because currently no reported ambient MSIA concentrations in the marine boundary exist, initial MSIA concentrations in the reaction medium were selected between 10 and 1300 μM, corresponding to 0.001–0.13 nmol (m^3 air)$^{-1}$. These numbers are in the range of what is expected from observed DMSO concentrations assuming steady state conditions for MSIA with •OH as the oxidant and $k_{DMSO,•OH} = 4.5 \times 10^9$ M^{-1} s^{-1} and $k_{MSIA,•OH} = 1.2 \times 10^{10}$ M^{-1} s^{-1} (*12*):

$$k_{DMSO,•OH}[DMSO] = k_{MSIA,•OH}[MSIA] \Rightarrow [MSIA] = \frac{k_{DMSO,•OH}}{k_{MSIA,•OH}}[DMSO] = 0.38[DMSO] \quad (1)$$

The reaction medium was stirred throughout the 6-h experiment, and at selected time intervals, aliquots of solution were withdrawn, filtered through a polysulfone Acrodisc syringe filter (0.45 μm pore size, PALL Corp.), and analyzed for Fe(II), Fe(III), H_2O_2, and sulfur reactants and products. The pH of the reaction medium was measured prior to light exposure and after completion of the experiment. Control experiments were run for comparison.

Analytical Methods. Fe(II) concentrations were determined with UV–vis absorption (Ferrozine method) (*34*) and a Teflon Z-type flow cell (1 cm path length, FIAlab Instruments, Inc.) connected to a 5 W Xe lamp (FO-6000, WPI) and spectrometer (J&M TIDAS II, WPI). Fe(III) was measured analogously by prior reduction to Fe(II) with hydroxylamine hydrochloride (H_2NOH HCl, 99.9% purity, Aldrich) and subtraction of the previously determined Fe(II). A detection limit of 0.4 μM Fe(II) was obtained, and Fe(III) was below detection limit unless otherwise noted.

H_2O_2 was quantified directly with a H_2O_2 sensitive electrode (Apollo 4000, WPI). Standards ranging from 1 μM to 100 μM were prepared from a 30% (w/w) H_2O_2 stock (reagent grade, Mallinckrodt), and the detection limit was 2.8 μM.

Sulfur oxidation products were quantified using ion chromatography (IC) with electrochemical detection (see ref (*9*) for details). Detection limits were established at 1.2 μM for MSIA, 0.82 μM for MSA, 5.2 μM for hydroxymethane sulfinic acid (HMSIA), 6.1 μM for hydroxymethane sulfonic acid (HMSA), and 7.1 μM for SO_4^{2-}. Potential products HMSIA, HMSA, and SO_4^{2-} were below detection limits in all experiments.

Replicate experiments for each set of conditions were not feasible because of material and time constraints. However, the variability of results within the same ferrihydrite batch was established by conducting one representative experiment three times and assuming that standard deviations obtained in this manner are representative and transferable to other experiments. Relative standard deviations amount to less than 4%, 19%, 21%, 16%, and 2% for Fe(II) and Fe(III), H_2O_2, MSIA, MSA, and pH, respectively.

Results and Discussion

Photoproduction of Fe(II) in the Presence of DMSO, $DMSO_2$, MSIA, and MSA. Ferrihydrite used in photochemical experiments in Figure 1 was from one homogeneous batch. Fe(II) concentrations (Figure 1a) as a function of time are plotted as solid lines for individual experiments with added DMSO, $DMSO_2$, MSIA, and MSA. Dashed lines are light and dark controls, as indicated. Because dark controls with different sulfur species do not differ statistically, averaged values are plotted.

The most striking results are observed in the presence of MSIA where the initial Fe(II) photoproduction rate in solution is enhanced by a factor of 7.5 compared to the light control without sulfur species, 3.0×10^{-2} vs 0.4×10^{-3} μM s^{-1}, respectively. This increased rate of Fe(II) formation continues while MSIA is consumed and MSA formed until ~60 min, after which Fe(II) reaches steady state concentrations and MSA remains constant. Oxidation to SO_4^{2-} is not observed over the 6-h experiment. Although MSA appears to enhance Fe(II) formation in a separate ferrihydrite–MSA light experiment (downward pointing triangles), this effect is ascribed to the significantly lower pH (3.4–3.8) associated with the addition of MSA ($pK_a = 1$) (*35*), rather than a direct chemical reaction as confirmed by the constant MSA throughout the experiment. Lower pH facilitates dissolution of ferrihydrite which increases the photoactive $Fe(OH)^{2+}$ and stabilizes Fe(II) from reoxidation (*36*). Fe(III) concentrations in this experiment were above the detection limit, at 1 ± 0.4 μM, from

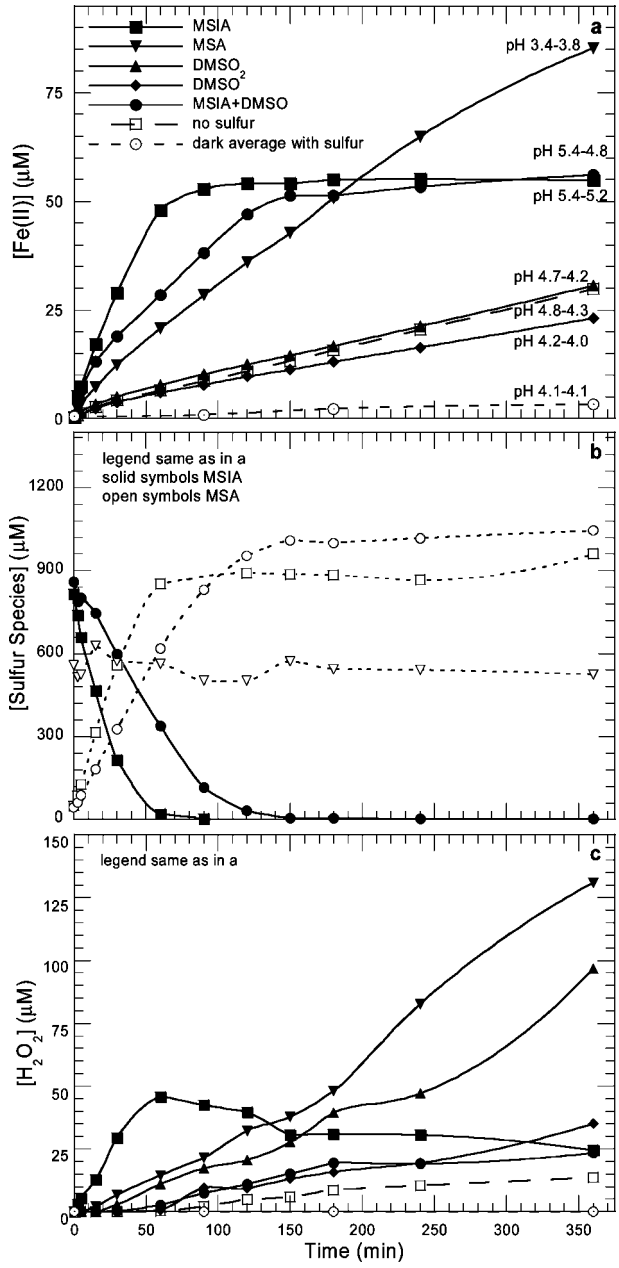

FIGURE 1. Results from photochemical experiments with one batch of ferrihyrdrite in the presence of DMSO, $DMSO_2$, MSIA, and MSA. a. Fe(II). b. Sulfur species, MSIA (solid symbols) and MSA (corresponding open symbols), c. H_2O_2. Initial and final pH values are noted near the end of each curve in part a. Results for iron light and dark controls are plotted in parts a and c with dashed lines, as indicated. Initial concentrations are reported in Table 1.

time 0 to 150 min, and then dropped below the detection limit, consistent with the observed pH increase (data not shown).

Note that the pH of MSIA containing solutions is above the control pH most likely because of ligand exchange on the ferrihydrite surface with MSIA that was added as its conjugate weak base ($pK_b = 11.7$ (*37*)). This ligand exchange is also confirmed by the lower-than-added measured initial aqueous MSIA concentrations of ~800 versus 1300 μM. Thus, the enhancing effect that MSIA has on the production of Fe(II) is not related to a pH change; if anything, the higher pH imparts a negative effect on the overall production of Fe(II) (vide infra).

$DMSO_2$ does not affect Fe(II) production, while DMSO seems to impart a weak inhibitory effect, even with a lower solution pH compared to the control. DMSO, due to its less polar nature, may preferentially adsorb to the ferrihydrite surface and in this way reduce the number of active sites available for photolysis. Potential oxidation products MSIA and SO_4^{2-} were not detected in either the $DMSO_2$ or the DMSO experiments, and although MSA was observed, it remained below the detection limit. The inhibiting effect of DMSO was also observed in the presence of MSIA (circles): initial Fe(II) production rates are identical to the corresponding MSIA only experiment (squares), but within 10 min the rate decreases. A similar pattern is observed for MSIA consumption and MSA production rates.

Concurrent H_2O_2 production (Figure 1c) is observed in all reactions except the dark controls. In the absence of other electron donors, Fe(III) on hydrated iron oxide surfaces and in solution (in particular $Fe(OH)^{2+}$, the primary species in solution between pH ~3 and pH 6, (*36*)), will undergo photochemically induced LMCT to produce Fe(II) and H_2O_2:

$$\equiv \mathrm{Fe(III)} - (\mathrm{OH})^- \text{ and } \mathrm{Fe(OH)}^{2+} \xrightarrow{h\nu} \mathrm{Fe(II)(aq)} + (1/2)\mathrm{H_2O_2} \quad (2)$$

In this process newly exposed Fe(III) hydrolyzes and contributes to further acidification of the solution. In the presence of MSIA, immediate H_2O_2 production (1.7×10^{-2} μM s^{-1} versus below detection limit for the control) stems from the disproportionation of hydroperoxy/superoxide radicals' ($HO_2^{\bullet}/O_2^{\bullet-}$) produced in the second oxidation of the intermediate MSIA radical with O_2 (see Figure 2 in ref (*9*)), analogous to the iron–oxalate system (*7, 8*). The net photochemical reaction consists of the irreversible oxidation of MSIA to MSA, the production of H_2O_2, and the reduction of surface iron with subsequent Fe(II) detachment from the surface in a slow process:

$$\equiv \mathrm{Fe(III)}{-}(\mathrm{OOSCH_3})^- + (1/2)\mathrm{O_2} + \mathrm{H_2O} \xrightarrow{h\nu} \mathrm{Fe(II)(aq)} + (\mathrm{CH_3SOOO})^- + (1/2)\mathrm{H_2O_2} + \mathrm{H}^+ \quad (3)$$

After MSIA depletion, H_2O_2 production from this process ceases and the Fenton reaction is responsible for the observed H_2O_2 drop and leveling of Fe(II):

$$\mathrm{Fe(II)(aq)} + \mathrm{H_2O_2} \rightarrow \mathrm{Fe(OH)}^{2+} + {}^{\bullet}\mathrm{OH} \quad (4)$$

Hydroxyl radical ($^{\bullet}$OH) is produced as soon as Fe(II) and H_2O_2 form and contributes to the efficient oxidation of MSIA and DMSO.

H_2O_2 production is not elevated in the experiment with MSIA and DMSO, thus indicating that DMSO directly or indirectly inhibits its buildup in solution. Enhanced H_2O_2 production in the presence of $DMSO_2$ is not yet understood.

Determination of MSIA–Fe Reaction Kinetics with Initial Rates. One homogeneous batch of ferrihydrite was exposed to varying amounts of initial MSIA concentrations ranging from 10 to 1300 μM (Figure 2, added MSIA concentrations are noted in μM in part a).

The initial rate of production of Fe(II) increases with initial MSIA concentration up to 500 μM MSIA. Higher MSIA concentrations do not lead to further Fe(II) rises (Figure 2a). MSIA to MSA conversion (Figure 2b), however, increases continually with initial MSIA concentrations, which is indicative of the presence of other process(es) (vide infra). In all experiments MSIA is consumed in approximately 90 min (see line in Figure 2). After 90 min, Fe(II) concentrations level off following the same trend as the light control (i.e., eq 2).

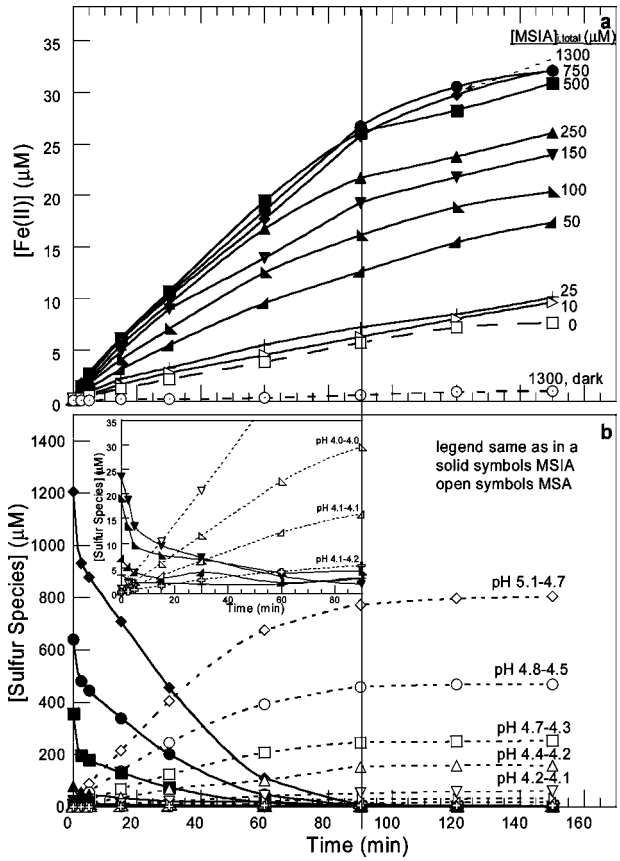

FIGURE 2. Results from photochemical experiments with one batch of ferrihydrite (different from that used in Figure 1) in the presence of varying concentrations of initial MSIA. a, Fe(II), light and dark controls in dashed lines, and b, sulfur species, MSIA (solid symbols) and MSA (corresponding open symbols). Initial MSIA concentrations are noted at the end of each curve in a. The vertical line indicates the 90 min mark.

A composite initial rate of Fe(II) production can be formulated by the sum of individual reaction rates from eqs 2 and 3: (i) the photolysis of hydrated Fe(III) in solution, $Fe(OH)^{2+}$, (ii) the photolysis of hydrated Fe(III) surface species, ≡Fe(III)−$(OH)^-$, and (iii) the LMCT with adsorbed MSIA, ≡Fe(III)−$(MSIA)^-$:

$$\left(\frac{d[Fe(II)]}{dt}\right)_i = k_1[Fe(OH)^{2+}_{aq}]_i + k_2[\equiv Fe(III)-OH]_i + k_3[\equiv Fe(III)-MSIA]_i^a \quad (5)$$

To determine the reaction rate constant, k_3, and reaction order, a, for the Fe–MSIA reaction, a set of initial assumptions are made: (i) Fe(II) oxidation mechanisms are neglected at time 0, because $[Fe(II)]_{t=0} = 0\ \mu M$, (ii) photolyses of hydrated Fe(III) species in solution and on the surface of ferrihydrite (first and second terms on the right-hand side of eq 5, respectively) are constant, and (iii) these two terms can be estimated from the initial rate of the control reaction without MSIA (justification of assumptions ii and iii is found in the Supporting Information (Supporting Material Text 1)). A corrected initial rate, defining Fe(II) production solely in terms of the Fe–MSIA reaction, can then be defined

$$\left(\frac{d[Fe(II)]}{dt}\right)_{i,corr} = k_3[\equiv Fe(III)-MSIA]_i^a \quad (6)$$

and rearranged

$$\log\left(\frac{d[Fe(II)]}{dt}\right)_{i,corr} = \log k_3 + a \log [\equiv Fe(III)-MSIA]_i \quad (7)$$

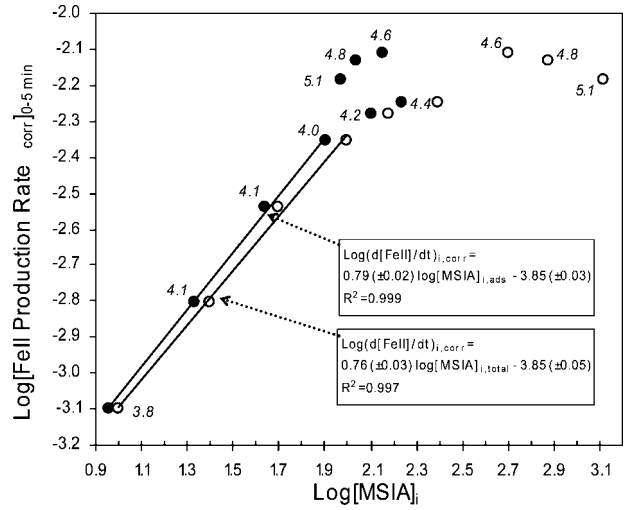

FIGURE 3. log[initial Fe(II) production rate (0–5 min) (μM s^{-1})] vs log[initial MSIA concentrations (μM)] for experiments plotted in Figure 2. Solid circles represent calculated adsorbed initial MSIA concentrationsb and open circles represent initial added total MSIA concentrations. Equations are for the solid lines as indicated. Numbers in italics show initial pH for the corresponding data pair.

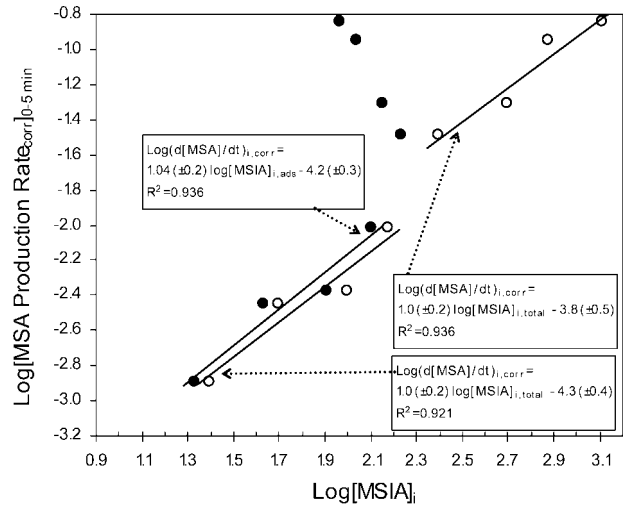

FIGURE 4. log[initial MSA production rate (0–5 min) (μM s^{-1})] vs log[initial MSIA concentrations (μM)] for experiments plotted in Figure 2. Solid circles represent calculated adsorbed initial MSIA concentrations, and open circles represent initial added total MSIA concentrations. Equations are for the solid lines as indicated.

A plot of the log of Fe(II) production rate against the log of adsorbed MSIA ($[\equiv Fe(III)-MSIA]_i = [MSIA]_{i,ads} = [MSIA]_{i,total} - [MSIA]_{i,aq}$; solid symbols in Figure 3) reveals the empirical rate constant, k_3 = antilog of the y-intercept, and order, a = slope, with regard to adsorbed MSIA. For reference, the rate is also plotted against total initial MSIA ($[MSIA]_{i,total}$; open symbols in Figure 3). Initial pH values are noted in italics.

A linear dependency is observed for both adsorbed and total MSIA at pH ≤ 4.1. At higher pH, the adsorbed data shows considerable scatter but follows the same overall trend, while for total MSIA deviation from linearity is observed. Student t tests reveal that the difference in slopes of the two least-squares fits is statistically insignificant and that a slope of 1 is within the 95% confidence interval of $a = 0.79 \pm 0.02$. Thus, it is likely that the reaction order with regard to MSIA is an underestimation due to the high probability of reoxidation of Fe(II) at the surface without detaching (*38*). The

pseudo-first-order empirical rate constants for both the adsorbed MSIA and the linear section of total MSIA are identical, $k_3 = 10^{-3.85}$ s^{-1} = 1.4 × 10^{-4} s^{-1}. Two additional ferrihydrite batches made from $Fe(ClO_4)_3 \cdot 6H_2O$ resulted in insignificantly different k_3 values, 1.0 × 10^{-4} s^{-1} and 1.2 × 10^{-4} s^{-1}, while another batch made with $Fe(NO_3)_3 \cdot 9H_2O$ displayed a significantly larger value of 2.4 × 10^{-4} s^{-1}. Although this enhanced reactivity in the presence of NO_3^- impurities was consistently observed, the data is inconclusive. Finally, all k_3 values are in the same range as those reported for a series of iron(oxy)hydroxides in the presence of carboxylic acid electron donors (*7, 39*).

Analogous data treatment is performed on the rate of MSA production defined in the following rate law:

$$\left(\frac{d[MSA]}{dt}\right)_i = k_4[MSIA]_{i,aq} + k_5[\equiv Fe(III)-MSIA]_i^b \quad (8)$$

The first term on the right-hand side is the photolysis of aqueous MSIA, and the second term represents the LMCT reaction under investigation. The rate constant for photolysis of MSIA, k_4, was estimated in independent experiments (not shown) to be 5.5 × 10^{-5} s^{-1}, which is comparable to a value of 3.0 × 10^{-5} s^{-1} reported by Bardouki et al. (*12*). Thus, from k_4 and measured aqueous MSIA concentrations, the contribution of MSA from photolysis can be estimated and extracted from the rate expression in eq 8, thereby delivering a corrected MSA production rate specific for the iron induced MSA formation:

$$\left(\frac{d[MSA]}{dt}\right)_{i,corr} = k_5[\equiv Fe(III)-MSIA]_i^b \quad (9)$$

As in eq 7 and Figure 3, the log of eq 9 allows for determination of both k_5 and b when plotting log of MSA formation vs log of adsorbed MSIA (Figure 4).

Consistent with Fe(II) production, two different regimes are identified. In the lower MSIA range, that is, pH ≤ 4.1, MSA production rate follows first order rate laws (slopes of 1.0) with almost identical rate constants, averaging $k_5 = 10^{-4.3}$ s^{-1} = 5.0 × 10^{-5} s^{-1}, with regard to both adsorbed and total MSIA. These rate orders and constants are within the 95% confidence interval of corresponding parameters for Fe(II) production. In the second regime, that is, pH > 4.1, MSA production decreases as a function of adsorbed MSIA but increases in relation to total MSIA (open symbols) in a first order rate law with rate constant $10^{-3.8}$. This rate constant is identical to the one determined for Fe(II) production. Observations suggest that iron induced MSIA oxidation to MSA occurs on the surface of ferrihydrite independent of the fraction of adsorbed MSIA and pH, perhaps due to the formation of an outer-sphere complex that does not lead to Fe(II) detachment but allows MSIA to be oxidized. In other iron(oxy)hydroxide systems such outer-sphere complexes are more prevalent than inner-sphere complexes with increasing pH (*40*). It can also not be ruled out that the direct photolysis of MSIA is estimated incorrectly, in particular at the higher MSIA concentrations where the two terms in eq 8 become of similar magnitude. Overall, however, MSIA photolysis is likely to be overpredicted because the photolysis rate was established in the absence of ferrihydrite, which modifies the amount of radiation reaching each molecule in the reaction medium.

Fe(II) production depends on both pH and MSIA adsorption because these two are linked in the current experiment: the pH increases with increasing total MSIA. However, the fraction of adsorbed MSIA decreases steeply after pH ~4.2, following an adsorption isotherm typical of controlled ligand binding to a hydrous oxide (see Supporting Information (Supporting Material Figure 2)). Therefore, at higher total MSIA concentrations, the suppression of adsorption due to elevated pH more than compensates for the increase of free MSIA.

Photoproduction of Fe(II) in the Presence of DMSO. Because MSIA has not been measured in the marine atmosphere but its immediate precursor, DMSO, has (*30*), its effect on iron dissolution was further investigated. Noteworthy results were only obtained with ferrihydrite made from $Fe(NO_3)_3 \cdot 9H_2O$ and in the presence of increased UVR (no AM1 filter, representing solar radiation outside the atmosphere, see Supporting Information (Supporting Material Figure 3) for data). This is likely attributable to the photolysis of NO_3^- (λ_{max} = 302 nm *41, 42*), a contaminant from insufficient purification of ferrihydrite, producing $^{\bullet}OH$ in the reaction medium. $^{\bullet}OH$, which is otherwise ubiquitous in the atmosphere, is in this way available to oxidize DMSO to MSIA (*12, 43*).

After an initial 60–180 min of Fe(II) inhibition, as seen for DMSO in Figure 1, abrupt increases of Fe(II) were preceded by enhanced MSIA, MSA, and H_2O_2 concentrations. H_2O_2 partakes in the Fenton reaction (eq 4) producing more $^{\bullet}OH$, which in turn facilitates DMSO oxidation to MSIA and further to MSA. In some instances, a steady state for Fe(II) set in after ~2.5 h, but MSIA and MSA continued to increase because of the large surplus of DMSO. As before, oxidation to SO_4^{2-} is not observed over the course of the experiment.

Atmospheric Relevance. Current results reveal significant Fe(II), MSA, and H_2O_2 increases from the Fe(III)–MSIA LMCT reaction at aqueous MSIA levels corresponding to atmospheric concentrations as low as ~1.0 pmol m^{-3}, a value that is the lower end of observed concentrations of its precursor DMSO (*30*) and one order of magnitude smaller than its oxidation product MSA (*24*). The contribution of this reaction is estimated to be substantial compared to other known Fe(II) sources in the remote marine atmosphere (i.e., LMCT between organic acids and iron(oxy)hydroxides *7, 39*). Given that rate constants for all these reactions are similar, the concentration of the respective electron donors becomes the determinant factor in the relative significance of each process. Far removed from continental sources, the primary source of organic acids is from phytoplankton emitted isoprene oxidation (*44*), while MSIA stems from oxidation of the comparatively larger amounts of DMS. Although, to our best knowledge, MSIA field concentrations have not been reported, modeling studies by Capaldo and Pandis (*45*) framed MSIA as a long-lived intermediate that is estimated to be present in the atmosphere in concentrations comparable to MSA and sometimes even higher (*46*). Thus, MSIA concentrations could be similar or larger than organic acids (*24, 32*) implying that the photochemical dissolution of Fe(III) with MSIA may play a significant role in the vast areas of the open ocean. The reason that MSIA has hitherto not been observed could be attributed to sampling and analytical artifacts. For instance, continuous collection of bulk aerosols containing low molecular weight organic acids (MSIA could be categorized as such) may lead to their subsequent volatilization, thus resulting in depletion of the compound. In terms of analysis, MSIA may have been mistaken as acetate, glycolate, or lactate, as all of these will coelute on the IC. Clearly, more work is necessary to optimize sampling protocols and develop new methods that will allow for the unequivocal determination of MSIA.

Furthermore, MSIA is likely to contribute to the chemical processing of iron in atmospheric dust particles through continuous reduction and reoxidation, which leads to a colloidal kinetically more labile iron(oxy)hydroxide that is more bioavailable to phytoplankton after precipitation into the ocean (*38*). This reaction also constitutes an efficient new mechanism for atmospheric H_2O_2 and MSA formation, the latter of which impacts the branching ratio between MSA

and SO_2 production with implications on CCN abundance and global climate (*14*). Thus, this mechanism will likely help explain current discrepancies in both marine atmospheric iron as well as sulfur models, where sources of Fe(II) and MSA have remained unidentified, respectively (*13, 16, 17, 47*).

Acknowledgments

This research was supported by National Science Foundation Advance Fellowship Grant ATM-0137891, National Park Service Cooperative Agreement H9453020047, and Central Washington University.

Supporting Information Available

Represeentative XRD scan of synthesized ferrihydrite, justification of assumptions ii and iii for eq 6, the adsorption isotherm for the ferrihydrite–MSIA system, and Fe(II), sulfur species, MSIA, and MSA concentrations in photochemical experiments with different batches of ferrihydrite that were all made with $Fe(NO_3)_3 \cdot H_2O$. This material is available free of charge via the Internet at http://pubs.acs.org.

Literature Cited

(1) Gao, Y.; Fan, S. M.; Sarmiento, J. L. Aeolian iron input to the ocean through precipitation scavenging: A modeling perspective and its implication for natural iron fertilization in the ocean. *J. Geophys. Res.* **2003**, *108*, 4221.

(2) Wells, M. L.; Price, N. M.; Bruland, K. W. Iron chemistry in seawater and its relationship to phytoplankton: a workshop report. *Mar. Chem.* **1995**, *48*, 157–182.

(3) Liu, X. W.; Millero, F. J. The solubility of iron in seawater. *Mar. Chem.* **2002**, *77*, 43–54.

(4) Barbeau, K.; Rue, E. L.; Trick, C. G.; Bruland, K. T.; Butler, A. Photochemical reactivity of siderophores produced by marine heterotrophic bacteria and cyanobacteria based on characteristic Fe(III) binding groups. *Limnol. Oceanogr.* **2003**, *48*, 1069–1078.

(5) Borer, P. M.; Sulzberger, B.; Reichard, P.; Kraemer, S. M. Effect of siderophores on the light-induced dissolution of colloidal iron(III) (hydr)oxides. *Mar. Chem.* **2005**, *93*, 179–193.

(6) Emmenegger, L.; Schoenenberger, R.; Sigg, L.; Sulzberger, B. Light-induced redox cylcing of iron in circumneutral lakes. *Limnol. Oceanogr.* **2001**, *46*, 49–61.

(7) Pehkonen, S. O.; Siefert, R.; Erel, Y.; Webb, S.; Hoffmann, M. Photoreduction of iron oxyhydroxides in the presence of important atmospheric organic compounds. *Environ. Sci. Technol.* **1993**, *27*, 2056–2062.

(8) Zuo, Y.; Hoigné, J. Formation of hydrogen peroxide and depletion of oxalic acid in atmospheric water by photolysis of iron(III)-oxalato complexes. *Environ. Sci. Technol.* **1992**, *26*, 1014–1022.

(9) Johansen, A. M.; Key, J. M. Photoreductive dissolution of ferrihydrite by methanesulfinic acid: Evidence of a direct link between dimethylsulfide and iron-bioavailability. *Geophys. Res. Lett.* **2006**, *33*, 4818.

(10) Sunda, W.; Kieber, D. J.; Kiene, R. P.; Huntsman, S. An antioxidant function for DMSP and DMS in marine algae. *Nature* **2002**, *418*, 317–320.

(11) Ravishankara, A. R.; Rudich, Y.; Talukdar, R.; Barone, S. B. Oxidation of atmospheric reduced sulphur compounds: Perspective from laboratory studies. *Philos. Trans. R. Soc. London, Ser. B* **1997**, *352*, 171–181.

(12) Bardouki, H.; da Rosa, M. B.; Mihalopoulos, N.; Palm, W. U.; Zetzsch, C. Kinetics and mechanism of the oxidation of dimethylsulfoxide (DMSO) and methanesulfinate (MSI-) by OH radicals in aqueous medium. *Atmos. Environ.* **2002**, *36*, 4627–4634.

(13) Lucas, D. D.; Prinn, R. G. Mechanistic studies of dimethylsulfide oxidation products using an observationally constrained model. *J. Geophys. Res.* **2002**, *107*.

(14) Charlson, R. J.; Lovelock, J. E.; Andreae, M. O.; Warren, S. G. Oceanic phytoplankton, atmospheric sulphur, cloud albedo and climate. *Nature* **1987**, *326*, 655–661.

(15) Schwertmann, U.; Cornell, R. M. *Iron Oxides in the Laboratory, Preparation and Characterization*; VCH Verlagsgesellschaft mbH: Weinheim, Germany, 1991.

(16) Luo, C.; Mahowald, N. M.; Meskhidze, N.; Chen, Y.; Siefert, R. L.; Baker, A. R.; Johansen, A. M. Estimation of iron solubility from observations and a global aerosol model. *J. Geophys. Res.* **2005**, *110*, 3307.

(17) von Glasow, R.; Crutzen, P. J. Model study of multiphase DMS oxidation with a focus on halogens. *Atmos. Chem. Phys.* **2004**, *4*, 589–608.

(18) Brunauer, S.; Emmett, P. H.; Teller, E. Adsorption of gases in multimolecular layers. *J. Am. Chem. Soc.* **1983**, *60*, 309–319.

(19) Leifer, A. *The kinetics of environmental aquatic photochemistry*; American Chemical Society: Washington, DC, 1988.

(20) Stumm, W.; Morgan, J. J. *Aquatic Chemistry: Chemical Equilibria and Rates in Natural Waters*, 3rd ed.; John Wiley & Sons: New York, 1996.

(21) von Glasow, R.; Sander, R. Variation of sea salt aerosol pH with relative humidity. *Geophys. Res. Lett.* **2001**, *28*, 247–250.

(22) Chen, Y.; Siefert, R. L. Determination of various types of labile atmospheric iron over remote oceans. *J. Geophys. Res.* **2003**, *108*, 4774.

(23) Chen, Y.; Siefert, R. L. Seasonal and spatial distributions and dry deposition fluxes of atmospheric total and labile iron over the tropical and subtropical North Atlantic Ocean. *J. Geophys. Res.* **2004**, *109*, 9305.

(24) Johansen, A. M.; Siefert, R. L.; Hoffmann, M. R. Chemical composition of aerosols collected over the tropical North Atlantic Ocean. *J. Geophys. Res.* **2000**, *105*, 15277–15312.

(25) Sciare, J.; Baboukas, E. D.; Kanakidou, M.; Krischke, U.; Belviso, S.; Bardouki, H.; Mihalopoulos, N. Spatial and temporal variability of atmospheric sulfur containing gases and particles during the Albatross campaign. *J. Geophys. Res.* **2000**, *105*, 14,433–14,448.

(26) Jourdain, B.; Legrand, M. Seasonal variations of atmospheric dimethylsulfide, dimethylsulfoxide, sulfur dioxide, methanesulfonate, and non-sea-salt sulfate aerosols at Dumont d'Urville (coastal Antarctica) (December 1998 to July 1999). *J. Geophys. Res.* **2001**, *106*, 14391–14408.

(27) Legrand, M.; Sciare, J.; Jourdain, B.; Genthon, C. Subdaily variations of atmospheric dimethylsulfide, dimethylsulfoxide, methansulfonate, and non-sea-salt sulfate aerosols in the atmospheric boundary layer at Dumont d'Urville (coastal Antarctica) during summer. *J. Geophys. Res.* **2001**, *106*, 14,409–14,422.

(28) Davis, D.; Chen, G.; Kasibhatla, P.; Jefferson, A.; Tanner, D.; Eisele, F.; Lenschow, D.; Neff, W.; Berresheim, H. DMS oxidation in the Antarctic marine boundary layer: Comparison of model simulations and field observations of DMS, DMSO, $DMSO_2$, H_2SO_4. (g), MSA(g), and MSA(p). *J. Geophys. Res.* **1998**, *103*, 1657–1678.

(29) Nowak, J. B.; Davis, D. D.; Chen, G.; Eisele, F. L.; Mauldin, R. L., III; Tanner, D. J.; Cantrell, C.; Kosiciuch, E.; Bandy, A.; Thornton, D.; Clarke, A. D. Airborne Observations of DMSO, DMS, and OH at Marine Tropical Latitudes. *Geophys. Res. Lett.* **2001**, *28*, 2201–2204.

(30) Lee, P. A.; de Mora, S. J.; Levasseur, M. A Review of Dimethylsulfoxide in Aquatic Environments. *Atmos. Ocean* **1999**, *37*, 439–456.

(31) Berresheim, H.; Huey, J. W.; Thorn, R. P.; Eisele, F. L.; Tanner, D. J.; Jefferson, A. Measurements of dimethyl sulfide, dimethyl sulfoxide, dimethyl sulfone, and aerosol ions at Palmer Station, Antarctica. *J. Geophys. Res.* **1998**, *103*, 1629–1637.

(32) Johansen, A. M.; Siefert, R. L.; Hoffmann, M. R. Chemical characterization of ambient aerosol collected during the southwest-monsoon and inter-monsoon seasons over the Arabian Sea: Anions and cations. *J. Geophys. Res.* **1999**, *104*, 26325–26347.

(33) Johansen, A. M.; Hoffmann, M. R. Chemical characterization of ambient aerosol collected during the northeast monsoon season over the Arabian Sea: Anions and cations. *J. Geophys. Res.* **2004**, *109*.

(34) Stookey, L. L. Ferrozine-A new spectrophotometric reagent for iron. *Anal. Chem.* **1970**, *42*, 779–781.

(35) Barcellos da Rosa, M.; Elend, M.; Zetzsch, C. Some reactions of DMSO and MSIA in the aqueous phase of sea-spray: A contribution to CMD-APP and EC-project EL-CID, GSF-Forschungszentrum für Umwelt and Gesundheit, 2000, 131–135.

(36) Stumm, W.; Morgan, J. J. *Aquatic Chemistry*, 3rd ed.; John Wiley & Sons, Inc.: New York, 1996.

(37) Wudl, F.; Lightner, D. A.; Cram, D. J. Methanesulfinic Acid and Its Properties. *J. Am. Chem. Soc.* **1967**, *89*, 4099–4101.

(38) Moffett, J. W. In *The Biogeochemistry of Iron in Seawater*; Turner, D. R., Hunter, K. A., Eds.; John Wiley & Sons Ltd: Chichester, U.K., 2001; Vol. 7, pp 344–372.

(39) Suter, D.; Banwart, S.; Stumm, W. Dissolution of hydrous iron(III) oxides by reductive mechanisms. *Langmuir* **1991**, *7*, 809–813.

(40) Peak, D.; Sparks, D. L. Mechanisms of Selenate Adsorption on Iron Oxides and Hydroxides. *Environ. Sci. Technol.* **2002**, *36*, 1460–1466.

(41) Turnipseed, A. A.; Ravishankara, A. R. In *Dimethylsulfide: Oceans, Atmosphere and Climate*; Angeletti, G. R. a. G., Ed.; Kluwer Academic Publishers: Norwell, MA, 1993; pp 185–196.

(42) Arsene, C.; Barnes, I.; Becker, K. H. FT-IR product study of the photo-oxidation of dimethyl sulfide: Temperature and O-2 partial pressure dependence. *Phys. Chem. Chem. Phys.* **1999**, *1*, 5463–5470.

(43) Scaduto, R. C. Oxidation of DMSO and Methanesulfinic Acid by the Hydroxyl Radical. *Free Radical Biol. Med.* **1995**, *18*, 271–277.

(44) Yokouchi, Y.; Li, H. J.; Machida, T.; Aoki, S.; Akimoto, H. Isoprene in the marine boundary layer (Southeast Asian Sea, eastern Indian Ocean, and Southern Ocean): Comparison with dimethyl sulfide and bromoform. *J. Geophys. Res.* **1999**, *104*, 8067–8076.

(45) Capaldo, K. P.; Pandis, S. N. Dimethylsulfide chemistry in the remote marine atmosphere: Evaluation and sensitivity analysis of available mechanisms. *J. Geophys. Res.* **1997**, *102*, 23251–23267.

(46) Hertel, O.; Christensen, J.; Hov, O. Modelling of the end products of the chemical decomposition of DMS in the marine boundary layer. *Atmos. Environ.* **1994**, *28*, 2431–2449.

(47) Hand, J. L.; Mahowald, N. M.; Chen, Y.; Siefert, R. L.; Luo, C.; Subramaniam, A.; Fung, I. Estimates of atmospheric-processed soluble iron from observations and a global mineral aerosol model: Biogeochemical implications. *J. Geophys. Res.* **2004**, *109*, 5305.

ES071469Y